On the feasibility of N_2 fixation via a single-site Fe^{I}/Fe^{IV} cycle: Spectroscopic studies of $Fe^{I}(N_2)Fe^{I}$, $Fe^{IV}{\equiv}N$, and related species

Michael P. Hendrich[†‡], William Gunderson[†], Rachel K. Behan[§], Michael T. Green[‡§], Mark P. Mehn[¶], Theodore A. Betley[¶], Connie C. Lu[¶], and Jonas C. Peters[‡¶]

[†]Department of Chemistry, Carnegie Mellon University, Pittsburgh, PA 15213; [§]Department of Chemistry and Biochemistry and Molecular Biology, Pennsylvania State University, University Park, PA 16802; and [¶]Department of Chemistry and Chemical Engineering, Arnold and Mabel Beckman Laboratories of Chemical Synthesis, California Institute of Technology, Pasadena, CA 55455

Edited by Richard R. Schrock, Massachusetts Institute of Technology, Cambridge, MA, and approved August 29, 2006 (received for review May 30, 2006)

The electronic properties of an unusually redox-rich iron system, $[PhBP^{R}_3]Fe{-}N_x$ (where $[PhBP^{R}_3]$ is $[PhB(CH_2PR_2)_3]^-$), are explored by Mössbauer, EPR, magnetization, and density-functional methods to gain a detailed picture regarding their oxidation states and electronic structures. The complexes of primary interest in this article are the two terminal iron(IV) nitride species, $[PhBP^{iPr}_3]Fe{\equiv}N$ (3a) and $[PhBP^{CH2Cy}_3]Fe{\equiv}N$ (3b), and the formally diiron(I) bridged-Fe(μ-N_2)Fe species, $\{[PhBP^{iPr}_3]Fe\}_2(\mu\text{-}N_2)$ (4). Complex 4 is chemically related to 3a via a spontaneous nitride coupling reaction. The diamagnetic iron(IV) nitrides 3a and 3b exhibit unique electronic environments that are reflected in their unusual Mössbauer parameters, including quadrupole-splitting values of 6.01(1) mm/s and isomer shift values of −0.34(1) mm/s. The data for 4 suggest that this complex can be described by a weak ferromagnetic interaction ($J/D < 1$) between two iron(I) centers. For comparison, four other relevant complexes also are characterized: a diamagnetic iron(IV) trihydride $[PhBP^{iPr}_3]Fe(H)_3(PMe_3)$ (5), an $S = 3/2$ iron(I) phosphine adduct $[PhBP^{iPr}_3]FePMe_3$ (6), and the $S = 2$ iron(II) precursors to 3a, $[PhBP^{iPr}_3]Fe{-}Cl$ and $[PhBP^{iPr}_3]$Fe-2,3:5,6-dibenzo-7-aza bicyclo[2.2.1]hepta-2,5-diene (dbabh). The electronic properties of these respective complexes also have been explored by density-functional methods to help corroborate our spectral assignments and to probe their electronic structures further.

dinitrogen activation | high-valent iron | nitrogenase | high-valent iron nitride | spectroscopy

Biological nitrogen reduction is an unusually difficult biocatalytic transformation to study because the nitrogenase apparatus needs to be partially loaded with electron (and presumably proton) equivalents before substrate uptake can occur (1–6). Despite the abundant structural, spectroscopic, and biochemical data now available, we still do not know definitively which metal(s) initially bind(s) dinitrogen, what metal oxidation state(s) promote(s) binding, or which reduced nitrogenous intermediates are generated (e.g., N^{3-}, NH^{2-}, N_2H, N_2H_3, etc.) en route to ammonia formation. Among the various inorganic mechanisms for N_2 fixation that have been broadly considered, one interesting scenario is a Chatt-type N_2 reduction cycle (7) mediated by a single iron center. Indeed, such a scenario using a single metal center was proposed originally for the Mo site in the cofactor (7) and recently has been demonstrated for a Tris(amido)amine molybdenum system by Schrock and coworkers (8–12). For a related iron-mediated scheme (Fig. 1), a key assumption is that a single iron site can accommodate ligands as electronically distinct as π-acidic N_2, and π-basic nitride or imide (N^{3-} and NH^{2-}, respectively).

Although a catalytic Fe cycle has yet to be established with any small-molecule model system, there are numerous theoretical and biochemical articles implicating iron as the site of biological N_2 fixation (13–22), and iron is the only metal known to be common to all nitrogenases. Moreover, certain iron complexes do mediate the conversion of N_2 to NH_3 and N_2H_4, albeit in low yields (23, 24), and work by authors of this article has established that four-coordinate iron complexes can accommodate both N_2 and nitride N^{3-} at a single binding site. Indeed by using sterically encumbered electron-releasing Tris(phosphino)borate ligands of the type $[PhBP^{R}_3]$ (where $[PhBP^{R}_3]$ is $[PhB(CH_2PR_2)_3]^-$), examples of $[PhBP^{R}_3]Fe{-}N_x$ complexes have been characterized thoroughly in which a single iron center spans as many as five formal iron oxidation states (25–31). As shown in Fig. 1, an intriguing scenario for the Fe-mediated Chatt-type cycle implicates Fe(I) and Fe(IV) as limiting oxidation states. To explore the feasibility of these oxidation states in a pseudo-tetrahedral model system featuring N_2 and nitride ligand types, we report here detailed studies on the electronic properties of several related complexes with EPR and Mössbauer spectroscopy and magnetization. In particular, we examine the complexes $[PhBP^{R}_3]Fe^{IV}{\equiv}N$, $\{[PhBP^{iPr}_3]Fe^{I}\}_2(\mu\text{-}N_2)$ to explore whether the formal oxidation states that have been used to describe these redox-active iron complexes are valid representations.

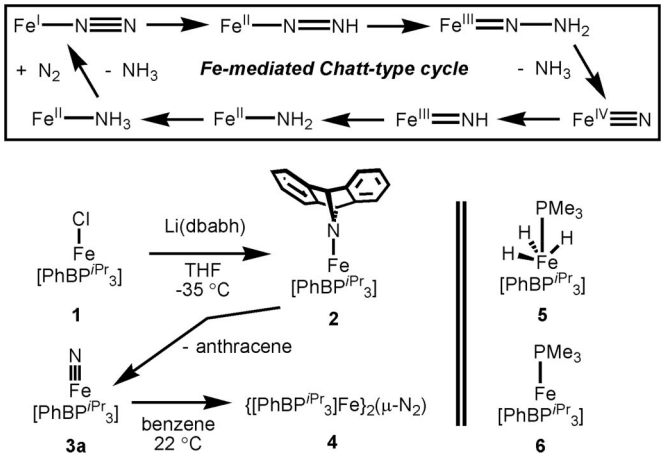

Fig. 1. A hypothetical Chatt-type Fe-mediated N_2 fixation cycle and complexes described herein.

Author contributions: M.P.H., M.T.G., and J.C.P. designed research; M.P.H., W.G., R.K.B., M.T.G., M.P.M., T.A.B., C.C.L., and J.C.P. performed research; M.P.H., W.G., R.K.B., M.T.G., M.P.M., and J.C.P. analyzed data; and M.P.H., M.P.M., and J.C.P. wrote the paper.

The authors declare no conflict of interest.

This article is a PNAS direct submission.

Abbreviation: dbabh, 2,3:5,6-dibenzo-7-aza bicyclo[2.2.1]hepta-2,5-diene.

[‡]To whom correspondence may be addressed. E-mail: hendrich@andrew.cmu.edu, mtg10@psu.edu, or jpeters@its.caltech.edu.

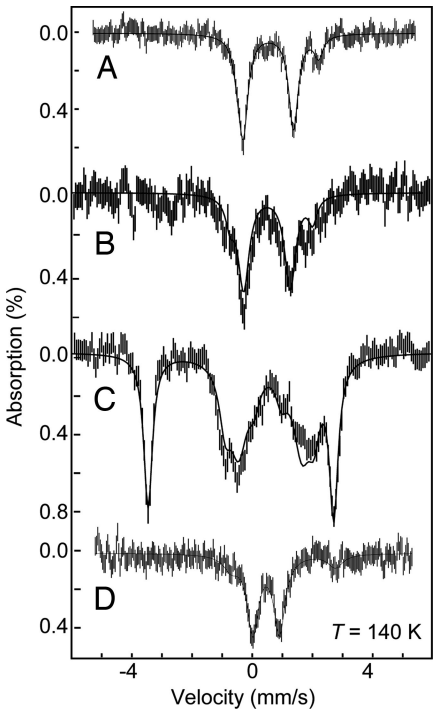

Fig. 2. Mössbauer spectra of THF solutions of 40 mM [PhBP$^{iPr}_3$]FeCl (**1**) (*A*); 40 mM [PhBP$^{iPr}_3$]Fe(dbabh) (**2**) (*B*); 40 mM [PhBP$^{iPr}_3$]Fe≡N (**3a**) (*C*); and 20 mM {[PhBP$^{iPr}_3$]Fe}$_2$(μ-N$_2$) (**4**) (*D*). All spectra were recorded at 140 K without an applied field. The short vertical lines are the experimental data, and the solid lines are fits using the parameters listed in Tables 1 and 3.

The nitride species [PhBP$^{iPr}_3$]Fe^{IV}≡N (**3a**) is generated by the addition of Li-2,3:5,6-dibenzo-7-aza bicyclo[2.2.1]hepta-2,5-diene (dbabh) to paramagnetic [PhBP$^{iPr}_3$]FeCl (**1**) at low temperature in THF (Fig. 1). This process generates the paramagnetic amide species [PhBP$^{iPr}_3$]Fe(dbabh) (**2**), which is thermally unstable and releases anthracene to afford diamagnetic **3a**. Nitride **3a** is itself thermally unstable and, at ambient temperature, dimerizes at an appreciable rate to produce the diiron(I) bridged-N$_2$ complex {[PhBP$^{iPr}_3$]Fe^{I}}$_2$(μ-N$_2$) (**4**). Characterization of the related nitride species, [PhBP$^{CH2Cy}_3$]Fe ^{IV}≡N (**3b**), also is described. For additional comparison, the tetravalent trihydride complex [PhBP$^{iPr}_3$]Fe(H)$_3$(PMe$_3$) (**5**) and the monovalent complex [PhBP$^{iPr}_3$]FePMe$_3$ (**6**) similarly have been examined. Crystal structures for **1**, **4**, **5**, and **6** have been described elsewhere (29–31).

Results

Mössbauer spectra of **1**–**4** in THF, recorded at 140 K in zero applied field, are shown in Fig. 2, and the parameters for each compound are summarized in Table 1. The parameters for the impurity species are summarized in Table 3, which is published as supporting information on the PNAS web site. In several cases, substantial impurities (≈20%) are observed by both Mössbauer and EPR spectroscopies, suggesting some degree of sample degradation via partial oxidation of the complexes in solution or during storage after freezing. Partial degradation of a frozen solution sample of an iron(I) complex also has been reported by Holland, Münck, and coworkers (32). The high-temperature Mössbauer spectrum of a sample of [PhBP$^{iPr}_3$]FeCl (**1**) (Fig. 2*A*) consists of two doublets. Complex **1** accounts for 80% of the Fe in the sample and has an isomer shift of $\delta = 0.58(2)$ mm/s and a quadrupole splitting $\Delta E_Q = 1.65(2)$ mm/s. The remaining 20% of the absorption arises from an unknown impurity species with parameters $\delta = 0.90(4)$ mm/s and $\Delta E_Q = 2.66(5)$ mm/s. The 4.2 K spectrum in a magnetic field of 45 mT (data not shown) displays significantly broader doublets for both species, typical of paramagnetic high-spin iron(II) centers in intermediate relaxation mode (33).

Table 1. Comparison of parameters for [PhBP$^R_3$]Fe complexes

Complex (spin)	D, cm^{-1}; E/D	δ, mm/s; ΔE_Q, mm/s
1 (2)	−8(2); 0.085	0.58(2); 1.65(2)
2 (2)	−8(2); 0.045	0.55(3); 1.75(4)
3a	—	−0.34(1); 6.01(1)
3b	—	−0.34(1); 6.01(1)
4 (3/2 × 3/2) $J = +4(1)$ cm^{-1}	−53(10); 0.10	0.53(3); 0.89(3)
5	—	0.01(2); 0.58(2)
6 (3/2)	+20(3); 0.16	0.57(2); 0.23(3)
[N$_3$N]Fe^{IV}CN*	—	−0.22; 3.28†
trans-[Fe(das)$_2$Cl$_2$]$^{2+}$	—	+0.12; 3.22‡
trans-[Fe(das)$_2$Br$_2$]$^{2+}$	—	+0.17; 3.16‡

das, *o*-phenylene-bis(dimethylarsine).
*[N$_3$N], [(*t*-BuMe$_2$SiNCH$_2$CH$_2$)$_3$N]$^{3-}$.
†Ref. 34.
‡Ref. 35.

The EPR spectra of the high-spin iron(II) complexes **1** and **2** are shown in Fig. 3. The low-temperature parallel mode (15 K, $\mathbf{B_1} \parallel \mathbf{B}$) EPR spectrum of **1** (40 mM in THF) shows a broad signal at $g = 12$ (Fig. 3*A*); no other signals are observed up to 1,000 mT. In perpendicular mode ($\mathbf{B_1} \perp \mathbf{B}$), the signal is significantly broader and approximately three times less intense. The dashed line in Fig. 3*A* is a simulation for an $S = 2$ species accounting for 70% of the spin in the sample. The parameters determined from the simulation and its temperature dependence are $D = -8(2)$ cm^{-1}, $E/D = 0.085$, and $g_z = 2.4$. The values are indicative of a high-spin iron(II) species having significant rhombic distortion and are consistent with the major species observed in the Mössbauer spectrum. The minority

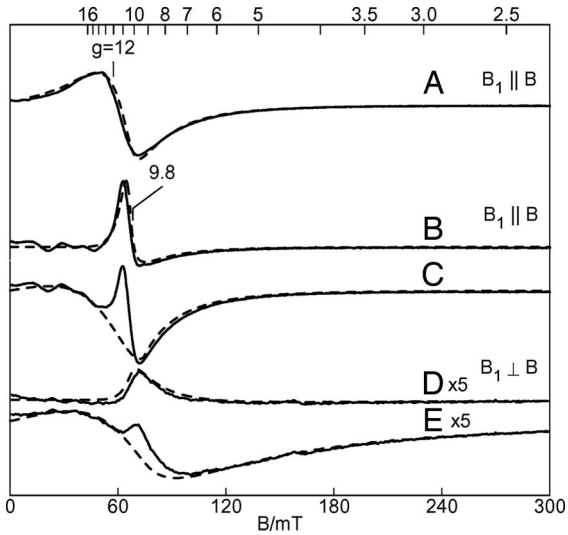

Fig. 3. EPR spectra ($T = 15$ K) of complexes in THF of 40 mM [PhBP$^{iPr}_3$]FeCl (**1**) ($\mathbf{B_1} \parallel \mathbf{B}$) (*A*); 40 mM [PhBP$^{iPr}_3$]Fe(dbabh) (**2**) after subtraction of minor species ($\mathbf{B_1} \parallel \mathbf{B}$) (*B*); 40 mM [PhBP$^{iPr}_3$]Fe(dbabh) (**2**) in THF ($\mathbf{B_1} \parallel \mathbf{B}$) without subtraction of the minor species (*C*); 40 mM [PhBP$^{iPr}_3$]Fe(dbabh) (**2**) in THF ($\mathbf{B_1} \perp \mathbf{B}$) after subtraction of minor species (*D*); and 40 mM [PhBP$^{iPr}_3$]Fe(dbabh) (**2**) in THF ($\mathbf{B_1} \perp \mathbf{B}$) without subtraction of the minor species (*E*). The solid lines are the experimental data, and the dashed lines are simulations using the following parameters. (*A*) $g_z = 2.4$, $D = -8$ cm^{-1}, $E/D = 0.085$. (*B* and *D*) $g_z = 2.5$, $D = -8$ cm^{-1}, $E/D = 0.045$. (*C* and *E*) Minority species: $S = 2$, $D = -8$ cm^{-1} (assumed), $E/D = 0.11$, $g_z = 2$. Spectral parameters: microwaves, 9.38 GHz ($\mathbf{B_1} \parallel \mathbf{B}$), 9.65 GHz ($\mathbf{B_1} \perp \mathbf{B}$), 0.2 mW.

species (30%) apparently has zero-field energies that render it unobservable with X-band EPR (36).

Metathesis of **1** with Li(dbabh) at low temperature in THF generates the iron amide [PhBP$^{iPr}_3$]Fe(dbabh) (**2**). Complex **2** is thermally unstable but has been detected previously by ^{1}H NMR and optical spectroscopies (30). A manganese analogue that we presume to be isostructural to **2** has been characterized thoroughly, including an x-ray diffraction analysis. The iron(II) amide **2** exhibits a doublet that accounts for ≈80% of the total Fe in the sample, with parameters $\delta = 0.55(3)$ mm/s and $\Delta E_Q = 1.75(4)$ mm/s (Fig. 2*B*). Approximately 20% of the absorption is from a presumed degradation product with parameters $\delta = 0.72(5)$ mm/s and $\Delta E_Q = 3.10(5)$ mm/s. Both species have parameters that are typical of high-spin Fe^{II} complexes. The Mössbauer spectrum at 4 K and 45 mT shows broad features indicative of a paramagnetic species, in addition to a small amount (<5%) of the nitride complex [PhBP$^{iPr}_3$]Fe≡N (**3a**) (see below).

The perpendicular mode EPR spectrum of **2** (40 mM in THF) shows a feature near $g = 9.8$ on top of a broader feature (Fig. 3*E*).[††] In parallel mode (Fig. 3*C*), both features near $g = 9.8$ sharpen and intensify. The signals near $g = 9.8$ can be quantitatively simulated with two Fe(II) species having concentrations of 28 mM (70%) and 12 mM (30%). The dashed lines in Fig. 3 *C* and *E* are simulations for the minor $S = 2$ species with parameters as given in the figure legend. The solid lines in Fig. 3 *B* and *D* are the experimental spectra after subtraction of the simulation of this minor component. The major species is simulated (dashed lines, Fig. 3 *B* and *D*) as an $S = 2$ iron(II) species with $D = -8(2)$ cm^{-1}, $E/D = 0.045$, and $g_z = 2.5$. The spin states and relative ratios of these species are in agreement with those observed in the Mössbauer sample of **2**.

Nitride **3a** was prepared by allowing a sample of **2** to thermally decay at 25°C over a period of minutes. Because **3a** is itself thermally unstable (decaying to {[PhBP$^{iPr}_3$]Fe}$_2$(μ-N$_2$) (**4**) over a period of minutes at 40 mM at room temperature), preparing a high-purity sample of **3a** at such high concentrations is difficult. The Mössbauer spectrum ($T = 140$ K) of **3a** in THF, generated from a 40 mM original stock solution of **1** and Li(dbabh), is shown in Fig. 2*C*. This spectrum contains a mixture of unresolved doublets from multiple species. We have attempted to fit this spectrum with combinations of **1**, **2**, and **4**; however, these combinations gave unsatisfactory fits. Instead, we must introduce two new impurities, which are presumably oxidation products, and a minor amount of **4**. Most important, however, is the observation of a prominent new doublet with parameters $\delta = -0.34(1)$ mm/s and $\Delta E_Q = 6.01(1)$ mm/s, which constitutes ≈35% of the iron in the sample. The spectrum of **3a** at 4 K in a magnetic field of 45 mT (Fig. 4*A*) shows that the inner doublets of the spectrum broaden, whereas the well resolved outer doublet is unchanged, consistent with paramagnetic impurities and a diamagnetic [PhBP$^{iPr}_3$]Fe≡N.

The chloride complex, [PhBP$^{CH2Cy}_3$]FeCl also reacts with Li(dbabh) to produce a related nitride species, [PhBP$^{CH2Cy}_3$]Fe≡N (**3b**). Unlike [PhBP$^{iPr}_3$]FeCl, the methylcyclohexyl-substituted derivative converts to the terminal nitride **3b** over several hours at temperatures below −50°C without observation of an intermediate Fe^{II}(dbabh) species. Additionally, although **3b** is unstable at temperatures above −50°C, it does not decay to a dinitrogen adduct species akin to **4**. It is therefore technically more straightforward to generate a highly concentrated sample of **3b** at low temperature than it is for **3a**. The Mössbauer spectrum of **3b** (Fig. 4*B*) exhibits an outer doublet that constitutes 75% of the iron in the sample with the same parameters as that observed for **3a**, corroborating their respective assignments. The remaining 25% of the iron originates from an unknown diamagnetic species, because the spectrum does not depend on the magnetic field, with parameters $\delta = 0.15(1)$ mm/s and $\Delta E_Q = 1.65(1)$ mm/s.

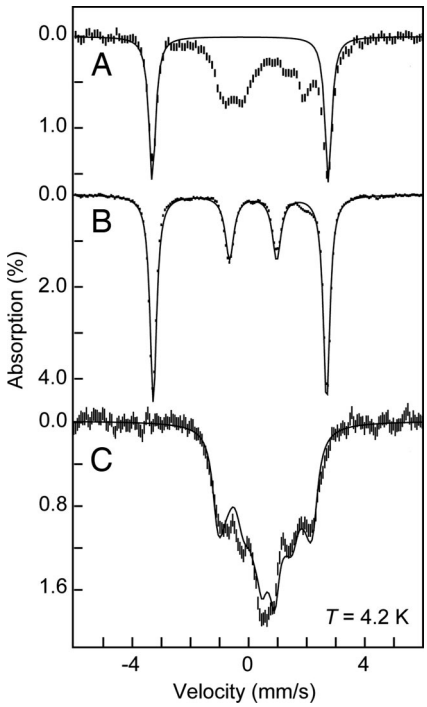

Fig. 4. Mössbauer spectra of 40 mM [PhBP$^{iPr}_3$]Fe≡N in THF (**3a**) (*A*); 40 mM [PhBP$^{MeCy}_3$]Fe≡N (**3b**) in THF (*B*); and 46 mM [PhBP$^{iPr}_3$]FePMe$_3$ (**6**) in toluene (*C*). All spectra are recorded at 4.2 K with a parallel applied field of 45 mT. The short vertical lines are the experimental data, and the solid lines are fits using the following parameters. (*A*) $\delta = -0.34(1)$ mm/s, $\Delta E_Q = 6.01(1)$ mm/s (35%). (*B*) Two species with $\delta = -0.34(1)$ mm/s, $\Delta E_Q = 6.01(1)$ mm/s (75%) and $\delta = 0.15(1)$ mm/s, $\Delta E_Q = 1.65(1)$ mm/s (25%). (*C*) $S = 3/2$, $D = 20$ cm^{-1}, $E/D = 0.16$, $g = 2.2$, $\delta = 0.57(2)$ mm/s, $\Delta E_Q = 0.23(3)$ mm/s, $A_x = A_y = 0$, $A_z = -8.8$ mT.

For comparison, we have collected Mössbauer spectra of diamagnetic [PhBP$^{iPr}_3$]Fe(H)$_3$(PMe$_3$) (**5**) (Fig. 7*A*, which is published as supporting information on the PNAS web site). Structural and NMR data rigorously established the presence of three classical hydride ligands for **5**, rather than an alternative hydride/dihydrogen adduct iron(II) formulation (31). Therefore **3a**, **3b**, and **5** each represent examples of formally iron(IV) species with diamagnetic ground states (30, 31). The $T = 140$ K Mössbauer spectrum of **5** shows a single quadrupole doublet with parameters $\delta = 0.01(2)$ mm/s and $\Delta E_Q = 0.58(2)$ mm/s. The $T = 4$ K spectrum at 45 mT of **5** is unchanged, consistent with its diamagnetic character.

The low-temperature EPR spectrum of a sample of **3a** (40 mM in THF) exhibits signals from the precursor **2** but with significantly lower intensities. The two species near $g = 9.8$ have decreased by 60%, and the $g = 1.95$ minor species is approximately the same (≈1% of sample). The EPR spectrum of **3b** shows very weak signals representing <1% of the total sample. These changes are consistent with the presence of the new diamagnetic Fe(IV) species observed in Mössbauer spectra.

Thermal decay of the nitride species **3a** (but not **3b**) affords a dinitrogen complex, {[PhBP$^{iPr}_3$]Fe}$_2$(μ-N$_2$) **4**. This complex has been characterized structurally and also can be prepared by Na/Hg amalgam reduction of **1** in THF (28). The Mössbauer spectrum of **4** ($T = 140$ K; Fig. 2*D*) can be fitted to two components: (*i*) a major species with parameters $\delta = 0.53(2)$ mm/s and $\Delta E_Q = 0.89(3)$ mm/s (80%) and (*ii*) a minor species with parameters $\delta = 1.10(4)$ mm/s and $\Delta E_Q = 3.50(4)$mm/s (20%) that appears to originate from an unknown iron(II) center. The spectrum at 4 K in a field of 45 mT (data not shown) exhibits a significantly broadened doublet

[††]A sharp feature at $g = 1.95$ originates from a minor $S = [1/2]$ species constituting 0.3 mM spins (≈1% of sample). This feature vanishes in parallel mode. No other signals are observed up to 1,000 mT.

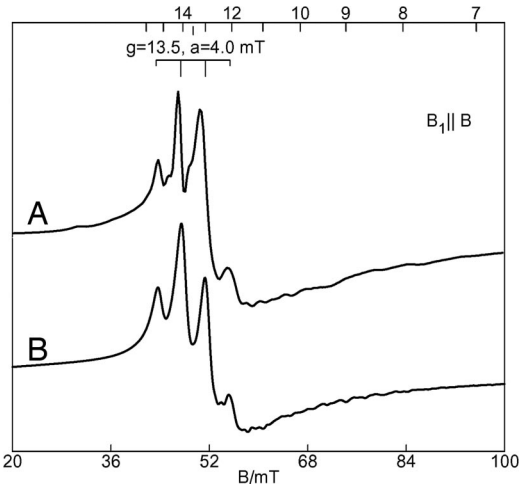

Fig. 5. EPR data for **4**. (*A*) EPR spectrum (T = 2.3 K, $\mathbf{B_1} \parallel \mathbf{B}$) of 20 mM {[PhBP$^{i\mathrm{Pr}}_3$]Fe}$_2$($\mu$-N$_2$) (**4**) in THF. (*B*) Simulation with parameters: $S_A = S_B = 3/2$, $J = +4$ cm^{-1}, $D_A = D_B = -53$ cm^{-1}, $E/D_A = E/D_B = 0.10$, $g_{Az} = g_{Bz} = 2.25$, $A_{Lz} = 77 \times 10^{-4}$ cm^{-1} (3 equivalent $I_L = 1/2$). Spectral parameters: microwaves, 9.38 GHz, 0.2 mW; modulation amplitude, 0.1 mT.

with the same parameters, indicative of a paramagnetic species in intermediate relaxation mode.

The low-temperature (2 K) parallel mode EPR spectrum of **4** (13 mM in THF) exhibits a prominent signal at $g = 13.5$ with a 1:3:3:1 hyperfine splitting pattern and $a = 4.0$ mT (Fig. 5*A*). The perpendicular mode spectrum shows a much broader feature near this same g value with 10-fold lower intensity.[‡‡] The simulation shown in Fig. 5*B* is for the ground doublet of a spin-coupled system $S_A = S_B = 3/2$ using the spin Hamiltonian of Eq. **1** (see *Supporting Materials and Methods*, which is published as supporting information on the PNAS web site). The parameters of the simulation are given in the figure legend. The exchange value (J) and axial zero-field splitting parameter ($D_A = D_B$) are determined from the magnetization data (see below). EPR simulations that match the spectra require a ferromagnetic interaction ($J > 0$) between the spins and site values of D_A, $D_B < 0$. In addition, the simulation is quantitative; the intensity of the simulation is in agreement with the sample concentration. To match the hyperfine splitting, the simulation includes three equivalent $I = 1/2$ nuclei with $A_z = 77 \times 10^{-4}$ cm^{-1}. The reason for the occurrence of the four-line pattern, instead of the expected seven-line pattern from the six equivalent phosphines, is as yet unclear. This value is unusually large for a ligand hyperfine coupling constant. The EPR signals of solutions of **4** change drastically at higher temperatures, and these changes will need to be explored further.

Isofield magnetization data were collected on a powder sample of **4** at magnetic fields of 0.5, 2.5, and 5.0 T. A plot of χT versus T of the data are shown in Fig. 8, which is published as supporting information on the PNAS web site. The data have been corrected for the following: diamagnetic susceptibility of **4** ($\chi_{\mathrm{dia}} = -8 \times 10^{-4}$ cm^3/mole), temperature-independent paramagnetism ($\chi_{\mathrm{TIP}} = +10 \times 10^{-4}$ cm^3/mole), and field-independent magnetization ($M_S = +8 \times 10^{-3}$ J/T per mole) (37, 38). The least-squares simulation of the data (solid line) is shown in Fig. 8 for two identical exchange-coupled $S = 3/2$ Fe(I) sites with $J = +4$ cm^{-1} and $D_A = D_B = -53$ cm^{-1}. For reference, the Brillouin curve ($D = 0, g = 2.0$) for an $S = 3$ state at 0.5 T also is shown. Simulations of the data with either an antiferromagnetic interaction ($J < 0$) or $D_A = D_B > 0$ did not fit the data.

[‡‡]The only other significant signal at 2 K is from a 1% minor species at $g = 2.05$ in perpendicular mode.

The complex [PhBP$^{i\mathrm{Pr}}_3$]FePMe$_3$ (**6**) (31) was studied, in part, as an aid to establish expected parameters for iron(I) complexes relevant for the present work. The Mössbauer spectrum of **6** in toluene, recorded at 140 K in zero applied field, is shown in Fig. 7*B*. The spectrum of **6** shows a single species with parameters $\delta = 0.57(2)$ mm/s and $\Delta E_Q = 0.23(3)$ mm/s. At 4 K and a field of 45 mT, the spectrum (Fig. 4*C*) shows a paramagnetic six-line pattern that can be fit with an $S = 3/2$ species having the highly anisotropic Fe hyperfine constants given in the figure legend. Interestingly, although the [PhBP$^{i\mathrm{Pr}}_3$]FePMe$_3$ complex has an isomer shift that is similar to that of the Fe(II) complexes **1** and **2**, the spin state $S = 3/2$ of [PhBP$^{i\mathrm{Pr}}_3$]FePMe$_3$ is indicative of an Fe(I) valence. To our knowledge, the Mössbauer parameters of only one other iron(I) coordination complex have been reported. The parameters of LFe$^{\mathrm{I}}$(HC≡CPh) (where L is HC(C[^{t}Bu]N-[2,6-diisopropylphenyl])$_2^-$) ($\delta = 0.44$ mm/s and $\Delta E_Q = 2.02$ mm/s) differ significantly, presumably because of the different geometric and electronic structure imposed by the β-diketiminate ligand and a symmetry that gives rise to an orbital degeneracy (32).

The low-temperature (15 K) perpendicular mode EPR spectrum of **6** exhibits a single signal with g values of 5.44 and 2.17 (see Fig. 9, which is published as supporting information on the PNAS web site). The simulation (dashed line) overlaid on the spectrum is for a paramagnetic center with $S = 3/2, D = +20(3)$ cm^{-1}, $E/D = 0.16$, and $g = 2.2$. The experimental spectrum is extremely broad, apparently because of molecular interactions. Consequently, the simulation does not match particularly well. The spin concentration based on the simulation is in approximate agreement with the sample concentration, and the spin state and amount are in agreement with the species observed in the Mössbauer sample. The spectrum does not show broadening for $T < 100$ K. Thus, the value of D was determined from a fit to the temperature dependence of the $S = 3/2$ signal. Importantly, with respect to the large hyperfine value observed for complex **4**, simulations of the EPR spectrum of **6** indicate that the signal is sufficiently broad to accommodate an unresolved hyperfine splitting of a magnitude similar to that observed for **4**. By contrast, there is no evidence for ^{31}P hyperfine in the EPR spectrum of $S = 2$ Fe(II)(dbabh) **2**. Simulations of the signal of **2**, which include three equivalent ^{31}P nuclei and a comparable large hyperfine A value, show an unmistakably large hyperfine splitting that is not observed in the experimental spectrum.

To aid in the analysis of these complexes, density-functional calculations were performed on **1**–**6**. Spin densities and Mössbauer parameters were determined by using both optimized and crystal structure geometries. Geometry optimizations were performed at the B3LYP/6–311G level. The same level of theory was used to determine electric field gradients for ΔE_Q and η. The Mulliken spin densities and Fe—X bond distances are listed in Tables 4 and 5, which are published as supporting information on the PNAS web site. The spin densities are in good agreement with the formal iron oxidation states of these species. Complexes **1** and **2**, which are each formally high-spin Fe(II), have 3.6 unpaired electrons, and the $S = 3/2$ Fe(I) centers in [PhBP$^{i\mathrm{Pr}}_3$]FePMe$_3$ and **4** each possess three unpaired spins. The closed shell singlets **3a** and [PhBP$^{i\mathrm{Pr}}_3$]Fe(H)$_3$(PMe$_3$) have no spin density. Differences between the spin densities obtained at the optimized and crystal structure geometries are negligible. Calculated bond distances are in reasonable agreement with experiment. The Fe—P bonds, however, appear to follow the general trend observed for second-row ligand donor atoms in that they are consistently (≈0.1-Å) too long.

There is generally good agreement between theory and experiment for **3a**, **4**, **5**, and **6** (Table 2). Differences in most cases are within the range of previously reported errors (39, 40). Interestingly, the Mössbauer parameters obtained from directly calculated crystal structure geometries are generally in better agreement with experiment than the parameters obtained from the density-functional

Table 2. Computationally predicted and experimentally observed Mössbauer parameters

		Experiment		Crystal structure			Optimized structure		
Complex	S	ΔE_Q	δ	η	ΔE_Q	δ	η	ΔE_Q	δ
1	2	1.65	0.58	0.55	3.18	0.48	0.15	3.18	0.59
2	2	1.75	0.55	0.71	−3.45	0.58	0.88	2.79	0.59
3	0	6.01	−0.34				0.01	6.22	−0.15
4	3/2	0.89	0.53	0.78	−1.32	0.49	0.78	−1.64	0.69
	3/2			0.90	1.37	0.49	0.58	−1.58	0.67
5	0	0.58	0.01	0.38	1.08	−0.05	0.66	1.05	0.13
6	3/2	0.23	0.57	0.68	−0.23	0.55	0.55	−0.20	0.80

method (DFT) optimized geometries. This finding may be a consequence of the inaccurately long Fe—P bond lengths obtained from density-functional methods. Although the isomer shifts calculated for **1** and **2** are in good agreement with experiment, their calculated ΔE_Q values have unusually large errors of ≈1.5 mm/s. These errors most likely result from our attempts to model the ground states of **1** and **2** as single determinant states. In both complexes, three electrons occupy the lowest two orbitals (e'') of the iron manifold. The correct description of these quintet ground states requires a linear combination of determinants in which both members of the e'' set are alternately doubly occupied. In contrast, the ground states of **3**, **4**, **5**, and **6** are well described by single determinants.

Discussion

In this study, we have used both physical and density-functional methods to explore whether the formal oxidation states Fe(I) and Fe(IV) are apt assignments for complexes such as the terminally bonded iron nitrides **3a** and **3b** and the diiron bridged-N_2 complex **4**. Such information is germane to our ongoing consideration of a hypothetical Fe(I)/Fe(IV) Chatt-type N_2 fixation cycle mediated by iron. The model complexes described in this article are unique in that they provide a synthetic platform in which an iron center can accommodate both N_2 and N^{3-} ligands at a single binding site. Such a feature would presumably be critical to a catalytic cycle that sampled intermediates bearing both types of ligand functionalities.

The crystallographic structures of $[BP_3]Fe{\equiv}N_x$ complexes show a pseudo-threefold symmetric environment with the borate, the Fe center, and the nitride or imide group lying along a common z axis (25, 27, 28, 41). Under this approximate C_{3v} symmetry, the d orbitals split into a low-lying nonbonding e set of dxy, dx^2–y^2 parentage (Fig. 6), an intermediate-energy a_1 orbital (dz^2-type), and a highest-energy e set of dxz, dyz parentage. Complexes **1** and **2** both are quintets ($S = 2$), and both exhibit Mössbauer parameters within the range expected for pseudo-tetrahedral high-spin Fe(II) complexes (33). From the EPR data, the zero-field terms for **2** are $D = -8\ cm^{-1}$ and $E/D = 0.085$. Under the symmetry C_{3v}, within the ^5D term, we derive from ligand-field theory the following approximate relations between the zero-field and orbital energies: $D = -\lambda^2(0.5/\Delta_{a1} + 1/\Delta_e)$, $E = \pm\ 0.5\lambda^2/\Delta_{a1}$. Here, Δ_e and Δ_{a1} are the energies from the ground orbital to the first and second excited orbitals, respectively. Using a spin-orbit constant of $\lambda = -100\ cm^{-1}$ for Fe(II), and the D and E values for **2**, gives $\Delta_e = 1{,}400\ cm^{-1}$ and $\Delta_{a1} = 7{,}400\ cm^{-1}$. The near-IR spectrum of **1** has a band at 7,360 cm^{-1} with an extinction coefficient of 100 $M^{-1}\ cm^{-1}$. The low extinction coefficient and the agreement in energy with the calculated value indicates that this is a d–d transition to the a_1 orbital (dz^2 parentage) lying above the nonbonding e set (dxy and dx^2–y^2 parentage).

The Mössbauer data obtained for the terminally bonded nitride complexes **3a** and **3b** are generally in agreement with the electronic structure picture that has been previously advanced (27, 30). For the

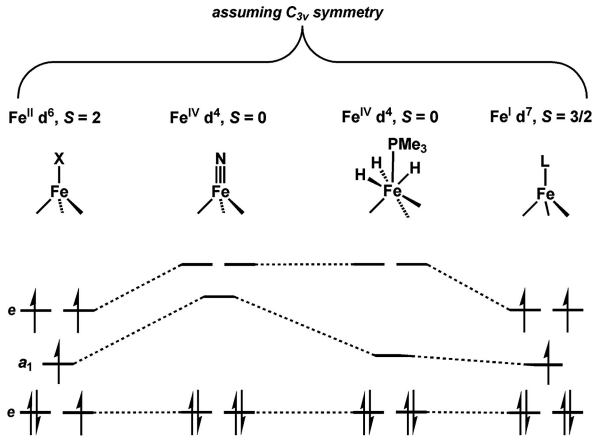

Fig. 6. Qualitative MO splitting diagrams to aid the discussion of the d-electron configurations for Fe(I), Fe(II), and Fe(IV) centers with the geometries described in this article.

nitride complex in the Fe(IV) oxidation state, density-functional methods predict four spin-paired electrons in the lower e set and an empty a_1 orbital with a highest occupied molecular orbital/lowest unoccupied molecular orbital (HOMO/LUMO) gap of almost 4 eV. This electronic structure is distinct from that of the trihydride complex $[PhBP^{iPr}_3]Fe(H)_3(PMe_3)$ **5**, in which an orbital of a_1 symmetry lies much closer to the lower e set. For comparison, the Mössbauer parameters for a few other low-spin Fe(IV) complexes are given in Table 1. The Tris(amido)amine Fe^{IV}—CN complex of Schrock has a significantly negative isomer shift and large quadrupole splitting. Wieghardt and coworkers (42, 43) have characterized two $S = 3/2$ Fe(V)—nitrido complexes at very low temperatures with $\delta = -0.04$ mm/s, ΔE_Q values −1.90 to −1.0 mm/s, and μ-N bridged complexes having an $S = 1$ Fe(IV) center $\delta = +0.04$ to +0.14 mm/s and ΔE_Q values between 0.79 and 1.13 mm/s. Interestingly, the large quadrupole-splitting parameter observed for **3a** and **3b** is larger than those of any other Fe^{IV} species and, to our knowledge, the largest of any known diamagnetic Fe complex. The geometry of the complexes places the hard nitride and borate functionalities along a pseudo-threefold z axis and polarizable phosphines around the periphery of the complex. This situation generates an unusually large electric field gradient along the z axis and, consequently, a large quadrupole splitting. In complex **5**, the anionic charges are more symmetrically disposed, implying an isotropic electric field gradient relative to that for **3a** or **3b** and, consequently, a much smaller quadrupole-splitting parameter.

The electronic description of the dinitrogen adduct **4** remains somewhat more enigmatic. The crystal structure of **4** shows a relatively short Fe—N distance of ≈1.82 Å and an N—N distance of 1.138(6) Å (30). These parameters reflect a degree of π-backbonding from iron into the N≡N π^* orbitals, but it is not so much as to suggest true electron transfer. For instance, the N—N distance in complexes featuring a bridged $N{=}N^{2-}$ ligand is expected to be closer to 1.24 Å (44). The N—N distance in **4**, however, is much shorter and is rather close to that of free N_2. The x-ray data are thus most indicative of an Fe(I) valence for each iron center of **4**, rather than an Fe^{II}—N=N—Fe^{II} formulation. Within the resolution of the Mössbauer spectrum, the iron sites of the dimeric complex **4** appear equivalent. Although the isomer shift often can be identified with a particular Fe valence state, similar isomer shifts are observed for the monomeric Fe(I) and Fe(II) complexes and for the dinitrogen adduct **4**. Thus, the isomer shift does not give a definitive indication of the iron valence for the highly covalent complexes described herein. The complementary EPR spectra that are provided are additionally informative and thus have helped to provide

a more complete picture of their appropriate spin and oxidation state assignments.

Although it is as yet unclear whether either of the idealized configurations, Fe^{I}—N≡N—Fe^{I} or Fe^{II}—N═N—Fe^{II}, accurately describes the electronic structure of **4**, they do provide an initial scheme for consideration of the magnetic information from the complex. As demonstrated above, the EPR and magnetization data of **4** support an Fe^{I}—N≡N—Fe^{I} electronic configuration. In particular, the least-squares simulation of the isofield magnetization data are appropriate for two identical exchange-coupled $S = 3/2$ Fe(I) sites with $J = +4\ cm^{-1}$ and $D_A = D_B = -53\ cm^{-1}$. We also have considered an alternative formulism representing the Fe^{II}—N═N—Fe^{II} configuration, wherein the identical Fe(II) sites have local spins of $S_A = S_B = 2$, and two electrons are assumed to be localized on the bridging dinitrogen to give a local dinitrogen spin of $S_C = 1$. For this three-spin model, an antiferromagnetic interaction between both iron centers to the central NN spin produces a ground system spin $S_S = 3$. Simulations of the magnetization data were extensively examined for the symmetric linear, three-spin model, with strong antiferromagnetic interactions, $J_{AC} = J_{BC} < -50\ cm^{-1}$, and weak exchange, $|J_{AB}| < 5\ cm^{-1}$, with values of $|D_A = D_B|$ ranging up to $100\ cm^{-1}$ and $g_A = g_B$ values between 2 and 2.5. The C site is representative of an $N{=}N^{2-}$ triplet with $D_C = 0$ and $g_C = 2$. The simulation routine, which we have written, calculates the magnetic moment from full diagonalization of the three-spin Hamiltonian, including zero-field terms. A suitable fit to the magnetization data for the three-spin model over this entire range of parameters could not be found.

In addition, the unusually large magnitude of the ^{31}P hyperfine coupling observed for **4** is indicative of strongly covalent Fe—P interactions and consistent with an Fe(I) valence state. This hyperfine splitting is not observed from the Fe(II) complex **2** but may be present in the Fe(I) complex **6**. A significantly larger hyperfine constant for an Fe(I) valence may be attributed to a higher degree of π-backbonding from the iron center into the phosphines for the Fe(I) valence relative to Fe(II). We cannot yet explain the appearance of a 1:3:3:1 ^{31}P hyperfine coupling pattern for **4**, rather than a seven-line pattern because of six equivalent Fe—P interactions. Currently, we can only speculate that this may be a dynamic effect correlated to the lifetime of the ^{31}P nuclear states. We have considered the possibility that the hyperfine pattern is caused by two equivalent ^{14}N nuclei in the three-spin formulism of the Fe(II)—N═N—Fe(II) configuration. Two observations argue strongly against this. First, even if the fifth line is missing (although we believe not), two equivalent ^{14}N nuclei would require a five-line 1:2:3:2:1 pattern, which gives poor simulations of the EPR spectrum. Second, the hyperfine constant of the ^{14}N nucleus derived from vector coupling of the three-spin model is $A_N = -4A_{S=3}$, giving a site value of $A_N = 160 \times 10^{-4}\ cm^{-1}$. This value is eight times greater than that observed for $NO^{\bullet}$ or $N_2^{-\bullet}$. Future work will benefit from ^{15}N isotopes to verify the conclusion.

Given all of the data presently available, we prefer an Fe(I) oxidation state assignment for **4** as most appropriate. Interestingly, Holland has prepared a diiron bridged-N_2 complex supported by β-diketiminate ligands, also with an $S = 3$ ground state (45). For this system, an iron(I) formulation also can be posited. However, the N—N bond distance that has been determined is more significantly elongated (1.18 ± 0.01 Å) relative to free N_2 than in **4**. Given this observation, and the harder coordination environment present for this β-diketiminate diiron system, it has been advanced that the three-spin exchange model is most appropriate for an Fe(II)—N═N—Fe(II) complex (45). We suspect that the soft phosphine ligands used in our own studies help to provide access to lower valent iron(I) because of their π-acidity.

To conclude, a single iron site is able to support terminally bonded N_2 and nitride (N^{3-}) ligands and also can accommodate a range of multielectron redox reactions. These features are requisite for the development of a single-site Fe-mediated N_2 fixation scheme based on the classic Chatt-type cycle. We also are considering mechanisms that would be initiated by a single iron site but that might thereafter sample bimetallic intermediates, such as diiron μ-N^{3-} and μ-NH^{2-} species. Ongoing work therefore includes the preparation and physical characterization of examples of such species (26, 27).

Materials and Methods

Complete materials and methods are provided in *Supporting Materials and Methods*.

Squid data were collected at the Molecular Materials Research Center of the Beckman Institute of the California Institute of Technology. This work was supported by National Institutes of Health Grant GM-070757 (to J.C.P.), Postdoctoral Fellowship GM-072291 (to M.P.M.), and Grant GM-077387 (to M.P.H.). R.K.B. is grateful for a Herman Frasch Foundation Fellowship, and M.T.G. acknowledges the Arnold and Mabel Beckman Foundation and the Alfred P. Sloan Foundation.

1. Burgess BK, Lowe DJ (1996) *Chem Rev* 96:2983–3011.
2. Eady RR (1996) *Chem Rev* 96:3013–3030.
3. Howard JB, Rees DC (1996) *Chem Rev* 96:2965–2982.
4. Thorneley RNF, Lowe DJ (1985) in *Molybdenum Enzymes*, ed Spiro TG (Wiley, New York), Vol 7, pp 221–284.
5. Dance I (2005) *J Am Chem Soc* 127:10925–10942.
6. Seefeldt LC, Dean DR (1997) *Acc Chem Res* 30:260–266.
7. Chatt J, Dilworth JR, Richards RL (1978) *Chem Rev* 78:589–625.
8. Yandulov DV, Schrock RR (2002) *J Am Chem Soc* 124:6252–6253.
9. Schrock RR (2003) *Chem Commun* 2389–2391.
10. Yandulov DV, Schrock RR (2003) *Science* 301:76–78.
11. Schrock RR (2005) *Philos Trans R Soc London A* 363:959–969.
12. Yandulov DV, Schrock RR (2005) *Inorg Chem* 44:1103–1117.
13. Barney BM, Laryukhin M, Igarashi RY, Lee H-I, Dos Santos PC, Yang T-C, Hoffman BM, Dean DR, Seefeldt LC (2005) *Biochemistry* 44:8030–8037.
14. Igarashi RY, Laryukhin M, Dos Santos PC, Lee H-I, Dean DR, Seefeldt LC, Hoffman BM (2005) *J Am Chem Soc* 127:6231–6241.
15. Barney BM, Yang T-C, Igarashi RY, Dos Santos PC, Laryukhin M, Lee H-I, Hoffman BM, Dean DR, Seefeldt LC (2005) *J Am Chem Soc* 127:14960–14961.
16. Lee H-I, Benton PMC, Laryukhin M, Igarashi RY, Dean DR, Seefeldt LC, Hoffman BM (2003) *J Am Chem Soc* 125:5604–5605.
17. Lee H-I, Hales BJ, Hoffman BM (1997) *J Am Chem Soc* 119:11395–11400.
18. Yang T-C, Maeser NK, Laryukhin M, Lee H-I, Dean DR, Seefeldt LC, Hoffman BM (2005) *J Am Chem Soc* 127:12804–12805.
19. Vrajmasu V, Munck E, Bominaar EL (2003) *Inorg Chem* 42:5974–5988.
20. Huniar U, Ahlrichs R, Coucouvanis D (2004) *J Am Chem Soc* 126:2588–2601.
21. Kästner J, Blöchl PE (2005) *ChemPhysChem* 6:1724–1726.
22. Hinnemann B, Nørskov JK (2003) *J Am Chem Soc* 125:1466–1467.
23. Leigh GJ (1992) *Acc Chem Res* 25:177–181.
24. George TA, Rose DJ, Chang YD, Chen Q, Zubieta J (1995) *Inorg Chem* 34:1295–1298.
25. Brown SD, Betley TA, Peters JC (2003) *J Am Chem Soc* 125:322–323.
26. Brown SD, Mehn MP, Peters JC (2005) *J Am Chem Soc* 127:13146–13147.
27. Brown SD, Peters JC (2005) *J Am Chem Soc* 127:1913–1923.
28. Betley TA, Peters JC (2003) *J Am Chem Soc* 125:10782–10783.
29. Betley TA, Peters JC (2003) *Inorg Chem* 42:5074–5084.
30. Betley TA, Peters JC (2004) *J Am Chem Soc* 126:6252–6254.
31. Daida EJ, Peters JC (2004) *Inorg Chem* 43:7474–7485.
32. Stoian SA, Yu Y, Smith JM, Holland PL, Bominaar EL, Münck E (2005) *Inorg Chem* 44:4915–4922.
33. Munck E (2000) in *Physical Methods in Bioinorganic Chemistry*, ed Que L, Jr (University Science, Sausalito, CA), pp 287–319.
34. Cummins CC, Schrock RR (1994) *Inorg Chem* 33:395–396.
35. Paez EA, Oosterhuis WT, Weaver DL (1970) *J Chem Soc Chem Commun* 506–507.
36. Palmer G (2000) in *Physical Methods in Bioinorganic Chemistry*, ed Que L, Jr (University Science, Sausalito, CA), pp 121–185.
37. Carlin RL (1986) *Magnetochemistry* (Springer, Berlin).
38. Girerd J-J, Journaux Y (2000) in *Physical Methods in Bioinorganic Chemistry*, ed Que L, Jr (University Science, Sausalito, CA), pp 321–374.
39. Zhang Y, Mao JH, Godbout N, Oldfield E (2002) *J Am Chem Soc* 124:13921–13930.
40. Neese F (2003) *Curr Opin Chem Biol* 7:125–135.
41. Jenkins DM, Betley TA, Peters JC (2002) *J Am Chem Soc* 124:11238–11239.
42. Meyer K, Bill E, Mienert B, Weyhermuller T, Wieghardt K (1999) *J Am Chem Soc* 121:4859–4876.
43. Grapperhaus CA, Mienert B, Bill E, Weyhermuller T, Wieghardt K (2000) *Inorg Chem* 39:5306–5317.
44. MacKay BA, Fryzuk MD (2004) *Chem Rev* 104:385–401.
45. Stoian SA, Vela J, Smith JM, Sadique AR, Holland PL, Munck E, Bominaar EL (2006) *J Am Chem Soc* 128:10181–10192.